ORGANOMETALLICS

ARTICLE

pubs.acs.org/Organometallics

Assembly of Cyclometalated Platinum(II) Complexes via 1,1′-Bis(diphenylphosphino)ferrocene Ligand: Kinetics and Mechanisms

S. Masoud Nabavizadeh,*[,†] Hashem Amini,[†] Hamid R. Shahsavari,[†] Masoud Namdar,[†] Mehdi Rashidi,*[,†] Reza Kia,[‡] Bahram Hemmateenejad,[†] Mohsen Nekoeinia,[†] Alireza Ariafard,[§] Fatemeh Niroomand Hosseini,[⊥] Alireza Gharavi,[∥] Ali Khalafi-Nezhad,[†] Mohammad Taghi Sharbati,[∥] and Farhad Panahi[†]

[†]Department of Chemistry, College of Sciences, Shiraz University, Shiraz 71454, Iran

[‡]Department of Chemistry, Science and Research Branch, Islamic Azad University, Tehran, Iran

[§]Department of Chemistry, Faculty of Sciences, Central Tehran Branch, Islamic Azad University, Shahrak Gharb, Tehran, Iran

[⊥]Department of Chemistry, Islamic Azad University, Shiraz Branch, Shiraz 71993-37635, Iran

[∥]Department of Electrical and Computer Engineering, Photonics Lab, Shiraz University, Shiraz, Iran

Supporting Information

ABSTRACT: The kinetics and mechanism of the reaction of the cyclometalated complexes [PtAr(C−N)(SMe_2)], **1**, in which Ar is Ph, *p*-MeC_6H_4, or *p*-$MeOC_6H_4$, and C−N is either ppy (deprotonated 2-phenylpyridine) or bhq (deprotonated benzo-[*h*]quinoline), with 1,1′-bis(diphenylphosphino)ferrocene, dppf, were studied using UV−visible and ^{31}P NMR spectroscopies. When 0.5 equiv of dppf was added, the binuclear Pt(II) complex [Pt_2Ar_2(C−N)$_2$(μ-dppf)], **2**, was formed in a good yield. The complexes were fully characterized using multinuclear (^1H, ^{31}P, and ^{195}Pt) NMR spectroscopy, and the structure of complex [Pt_2(*p*-$MeOC_6H_4$)$_2$(bhq)$_2$(μ-dppf)], **2c′**·CH_2Cl_2, was further identified by X-ray crystallography. On the basis of low-temperature ^{31}P NMR studies involving the starting complex [Pt(*p*-MeC_6H_4)(ppy)(SMe_2)], **1b**, we suggest that dppf displaces the labile ligand SMe_2 to give an uncommon complex, [Pt(*p*-MeC_6H_4)-(ppy)(dppf-κ^1P)], **A**, in which dppf-κ^1P is a monodentate dppf ligand, which rapidly forms an equilibrium with the chelating dppf isomer complex [Pt(*p*-MeC_6H_4)(dppf)(ppy-κ^1C)], **B**, in which ppy-κ^1C is the deprotonated ppy ligand that is C-ligated with the dangling N atom. In the second step, **A** is reacted with the remaining second half of starting complex **1b** to give the final Pt(II)−Pt(II) binuclear complex [Pt_2(*p*-MeC_6H_4)$_2$(ppy)$_2$(μ-dppf)], **2b**. A competitive-consecutive second-order reaction mechanism was suggested for the reaction using chemometric studies, and the rate constants at 5 °C for first and second steps were estimated as $k_2 = 10.7 \pm 0.2$ L mol^{-1} s^{-1} and $k_2' = 0.68 \pm 0.05$ L mol^{-1} s^{-1}, respectively. When the starting complex [Pt(*p*-MeC_6H_4)(ppy)(SMe_2)], **1b**, was reacted with 1 equiv of dppf, similarly the complex **A**, in equilibrium with **B**, was formed first, with the rate constant at 5 °C being $k_2 = 10.5 \pm 0.5$ L mol^{-1} s^{-1}, estimated using UV−visible spectroscopy. Subsequently, however, **A** and **B** would slowly and reversibly react with each other to form a new species, **C**, the structure of which, on the basis of ^{31}P and ^{195}Pt NMR spectra, was proposed to be [(*p*-MeC_6H_4)(ppy)Pt-(μ-dppf)Pt(*p*-MeC_6H_4)(ppy-κ^1C)(dppf-κ^1P)]; the same results were obtained when more than 1, e.g., 2, equiv of dppf was used, with a similar rate constant of $k_2 = 10.6 \pm 0.6$ L mol^{-1} s^{-1}. The complexes **1b** and **2b** were shown to have some interesting photophysical properties as investigated by absorption and electroluminescence spectroscopies.

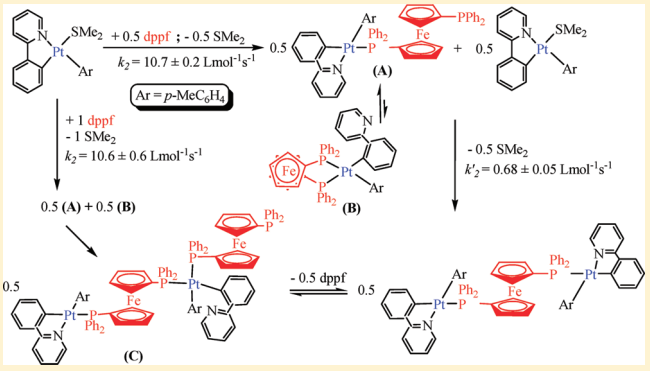

INTRODUCTION

There has been great interest in the synthesis and investigation of transition metal complexes containing the biphosphine ligand 1,1′-bis(diphenylphosphino)ferrocene, dppf, as the complexes have been involved in many catalysis, organic synthesis, electrochemical, materials science, and biological studies and applications.[1] This versatile ligand adopts various modes of coordination in order to match with the steric requirement dictated by the environment around the involved molecule.[2−5] The majority of the reported transition metal complexes with dppf are mononuclear complexes bearing a single or two chelating dppf ligands (see Scheme 1, I and II).[4,5a] Also, a third type of known coordination mode for dppf and related 1,1′-ferrocenyl diphosphines

Received: November 10, 2010
Published: February 16, 2011

Scheme 1. Some Coordination Modes of dppf

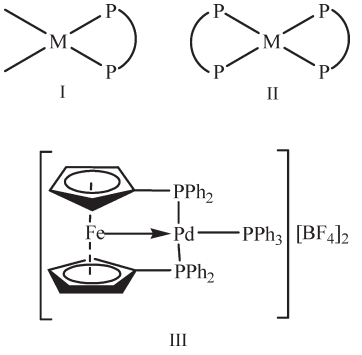

(especially with Pd and Pt), where the ligand prefers a *trans* coordination with a weak dative bond from iron, has been reported (see Scheme 1, III).[2b,c] However, diplatinum complexes containing bridging dppf are not common. We have recently reported some binuclear Pt(II) and Pt(IV) complexes, each having a dppf spacer ligand.[3a] In our recent report we have shown that the great chelating appetite of dppf has caused the rather strong cyclometalated chelate to open up from the N donor atom in the complex [PtMe(dppf)(ppy-κ^1C)], in which ppy = deprotonated 2-phenylpyridine.[3a]

In the present work, we have synthesized a series of cyclometalated diplatinum(II) complexes each containing a dppf spacer ligand, [$Pt_2Ar_2(C{-}N)_2(\mu$-dppf)], **2**, in which C−N is ppy or deprotonated benzo[*h*]quinoline (bhq) and Ar is a simple aromatic group, using a general synthetic approach involving the ligand replacement from the corresponding precursor having a labile ligand SMe_2. In fact this type of substitution procedure is the most common pathway used in the preparation of dppf complexes.[1] Due to the above-mentioned versatility of the dppf in complex formation, we were prompted to perform a systematic kinetic and mechanistic investigation on the related replacement reactions by using UV−visible and NMR spectroscopies (or chemometric methods in the case where 0.5 equiv of dppf was added) and to study the factors that control the reactivity of dppf complexes toward chelate opening. The presence of two cycloplatinated units in the same complex in compounds **2** may be very interesting in view of their potential applications in a wide variety of fields. It is well known that some platinacycles with C−N ligands have significant photophysical properties,[3b−i] and we indicated that the new complexes **2** appeared to probably be suitable candidates for further studies in these areas.

The crystal structure of the complex [$Pt_2(p$-$MeOC_6H_4)_2$-(bhq)$_2(\mu$-dppf)], **2c′**·CH_2Cl_2, is also reported. To the best of our knowledge this is the first X-ray structural determination of a diplatinum complex having an "open bridge" dppf ligand, although crystal structures of some transition metal complexes including dppf as bridging ligand have been reported.[5b−d] For example crystal structures for complexes [($C_6H_4CH_2NMe_2$-C2,N)$_2Pd_2Cl_2(\mu$-dppf)][5b] and [{Pd[5-(COH)C_6H_3C(H)=NCy-C2,N](Cl)}$_2(\mu$-dppf)][5c] have been reported with the conformations of the ferrocenyl skeleton being anticlinal eclipsed, although for a series of complexes with the general formula [($AuSC_6H_4${C(=O)Y}-2)$_2$-(μ-dppf)] the conformational modes adopted by the ferrocene cyclopentadienyl (Cp) rings are found as antiperiplanar staggered, synclinal eclipsed, and anticlinal staggered for Y = OH, NH_2, and N(H)Me, respectively.[5d]

Scheme 2

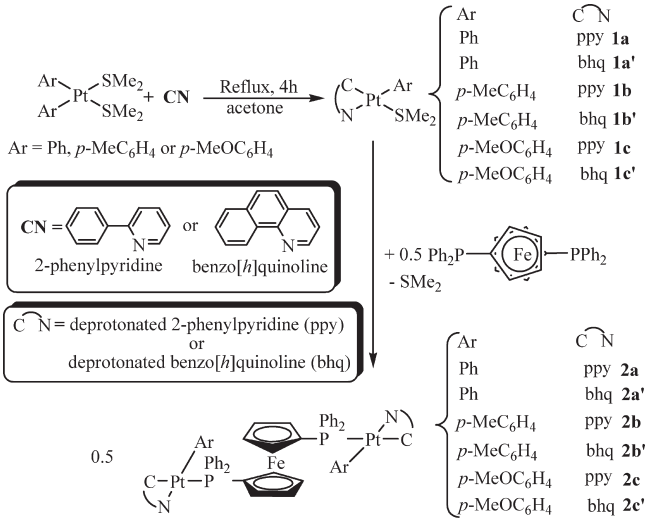

RESULTS AND DISCUSSIONS

Synthesis and Characterization of the Complexes. The general synthetic route to diplatinum complexes **2** is described in Scheme 2. The reaction of *cis*-[$PtAr_2(SMe_2)_2$], in which Ar = Ph, *p*-MeC_6H_4, or *p*-$MeOC_6H_4$, with 1 equiv of 2-phenylpyridine or benzo[*h*]quinoline, in refluxing acetone, gave the cyclometalated complexes [PtAr(C−N)(SMe_2)], **1**, in which C−N is either ppy or bhq. Reaction of each of the complexes **1** with 0.5 equiv of dppf, followed by replacement of the labile ligand SMe_2, yielded the diplatinum(II) complexes [$Pt_2Ar_2(C{-}N)_2(\mu$-dppf)], **2**, in a good yield.

The complexes **1** were characterized by their ^{1}H NMR spectra. In each case two well-defined peaks with a relative intensity 6:1 were observed, one for the terminal SMe_2 ligand (at δ = 2.2 ppm with $^3J_{PtH} \approx 25$ Hz) and the other for the H^6 proton, related to the CH group adjacent to ligating N atom of the C−N ligand (at δ = 8.8 ppm for ppy and δ = 9.1 ppm for bhq). The latter signal in each case is observed as a well-separated doublet due to coupling with the nearest H atom (H^5) with a $^3J_{H^6H^5}$ value close to 5.5 Hz, which is also weakly coupled to the platinum(II) center with a $^3J_{PtH^6}$ value around 17−19 Hz. The other C−N and Ar aromatic hydrogen atoms appeared at the expected regions, 7−9 ppm.

In the room-temperature ^{31}P NMR spectra of the binuclear complexes [$Pt_2Ar_2(C{-}N)_2(\mu$-dppf)], **2**, the observation of a sharp singlet signal for each of the analogues at a chemical shift of close to 20 ppm, which is accompanied by Pt satellites, confirms that the two PtAr(C−N) moieties, joined together by the dppf spacer ligand, are equivalent. The $^1J_{PtP}$ values for ppy complexes are close to 2000 Hz, while the $^1J_{PtP}$ values for bhq complexes are close to 2060 Hz. These $^1J_{PtP}$ values, which complied well with the values obtained from the corresponding ^{195}Pt NMR spectra, are within the expected range,[3a,5a] and the difference of ca. 3% is probably due to a greater *trans* influence of the metalated C atom of ppy derivatives as compared to that of the bhq analogues. In the ^{1}H NMR spectrum of each of the complexes **2**, the

dx.doi.org/10.1021/om101055n |*Organometallics* 2011, 30, 1466–1477

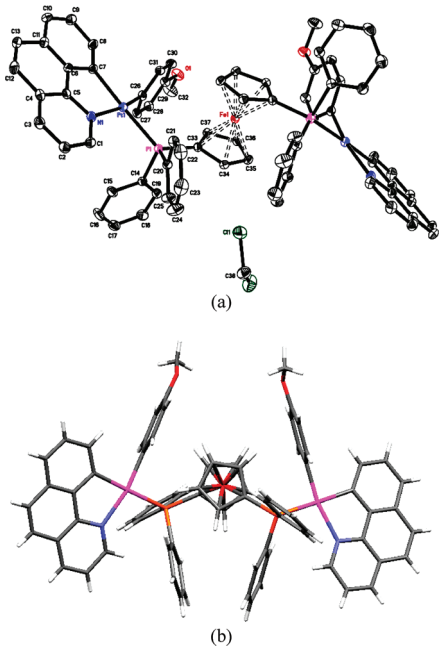

Figure 1. (a) Molecular structure of complex $[Pt_2(p\text{-}MeOC_6H_4)_2(bhq)_2(\mu\text{-}dppf)]$, $\mathbf{2c'}\cdot CH_2Cl_2$, showing 30% probability ellipsoids and the atomic numbering. The H atoms are omitted for clarity [symmetry operator for the unlabeled atoms: $-x+1, y, -z+0.5$]. Selected bond distances (Å) and angles (deg): Pt(1)−C(26), 2.013(6); Pt(1)−C(7), 2.052(7); Pt(1)−N(1), 2.162(6); Pt(1)−P(1), 2.3143(19); C(26)−Pt(1)−C(7), 90.4(3); C(26)−Pt(1)−N(1), 168.1(2); C(7)−Pt(1)−N(1), 79.7(3); C(26)−Pt(1)−P(1), 88.9(2); C(7)−Pt(1)−P(1), 177.6(2); N(1)−Pt(1)−P(1), 101.26(17). (b) Conformation of the cyclopentadienyl rings of the ferrocene moieties in complex **2c'**. The diagram highlights the relative dispositions of the five-membered rings as well as the relative orientations of the platinum atoms in the structure.

observation of a slightly broad singlet for either of the α- or β-protons, at δ values close to 4.4 or 3.4 ppm, respectively, confirms the equivalency of the two PtAr(C−N) moieties in the related complex. This is further confirmed by observation of only one signal for the two H^6 protons, related to the two CH groups adjacent to ligating N atoms of the two C−N ligands (appearing as a doublet signal at $\delta = 7.76$ ppm, for the ppy complexes, and at $\delta = 8.12$ ppm for the bhq complexes, with $^3J_{H^6H^5}$ and $^3J_{PtH^6}$ values close to 8 and 18.5 Hz, respectively); the signals appeared in a considerably lower field as compared to the other aromatic protons.

The structure of complex $[Pt_2(p\text{-}MeOC_6H_4)_2(bhq)_2(\mu\text{-}dppf)]$, $\mathbf{2c'}\cdot CH_2Cl_2$, was further determined by X-ray crystallography and is shown in Figure 1; the selected bond lengths and bond angles are also included in Figure 1. The geometry is best described as distorted square-planar, and the bond angles around the Pt center range from 79° to 101°. The chelating C−N bite angle, i.e., C(7)−Pt(1)−N(1), amounts to 79.7(3)°, which is significantly smaller than 90°, and implies that the chelate is probably under strain. The Cp(centroid)···Fe···Cp(centroid) twist angle of dppf is 132° (the angle has been determined as the torsion angle C33···Cp(centroid)1···Cp(centroid)2···C33A), and so dppf is arranged close to the "anticlinal eclipsed" conformation;[2a] the ideal torsion angle for this conformation is 144°. In the crystal structure, the molecules form 1-D infinite chains along the (1 0 1) direction by the intermolecular π−π interactions with the centroid (Cg1) to centroid (Cg2) distance of 3.696(4) Å; Cg1 and Cg2 are the centroid of the Pt1/N1/C5/C6/C7 and C4/C5/C6/C11/C12/C13 rings.

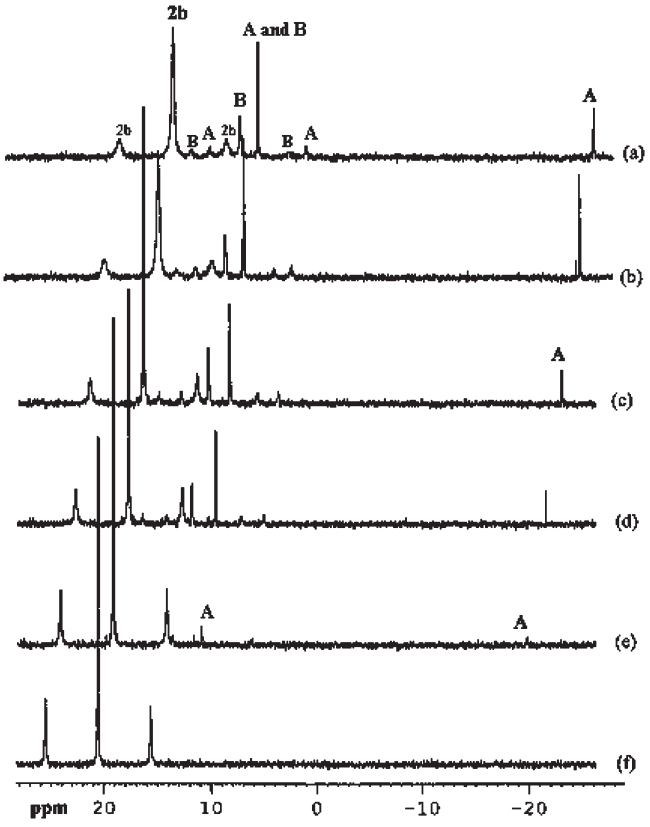

Figure 2. Changes in ^{31}P NMR spectra during the reaction of complex $[Pt(p\text{-}MeC_6H_4)(ppy)(SMe_2)]$, **1b**, with 0.5 equiv of dppf to form the binuclear complex $[Pt_2(p\text{-}MeC_6H_4)_2(ppy)_2(\mu\text{-}dppf)]$, **2b**, via the intermediate formation of complexes $[Pt(p\text{-}MeC_6H_4)(ppy)(dppf\text{-}\kappa^1P)]$, **A**, and $[Pt(p\text{-}MeC_6H_4)(dppf)(ppy\text{-}\kappa^1C)]$, **B**: (a) spectrum immediately after mixing the reactants at 233 K, (b) 9 min later at 233 K, (c) 23 min later at 248 K, (d) 31 min later at 258 K, (e) 41 min later at 273 K, (f) 50 min later at 298 K.

As discussed above, a sharp singlet was observed for the two equivalent phosphorus atoms in the room-temperature ^{31}P NMR spectrum of the binuclear complex $[Pt_2(p\text{-}MeC_6H_4)_2(ppy)_2(\mu\text{-}dppf)]$, **2b**. However, this singlet is considerably broadened when the spectrum is obtained at low temperatures (see Figure 2). It is probable that when a solid crystalline sample of complex **2b**, with its "anticlinal eclipsed" conformation, is dissolved in solvent, a fluxionality of the type shown in Scheme 3 occurs. As such, at room temperature the fluxionality behavior takes place very fast so that on average the "antiperiplanar staggered" conformation, with an ideal torsion angle of 180°, is observed, which gives rise to the observation of a sharp singlet in the ^{31}P NMR spectrum. At low temperatures however, the process is slow and both conformers are observable, leading to the observation of the broad singlet. It is therefore probable that the energy barrier to interconverting these eclipsed and staggered configurations is not high.

Mechanism of the Diplatinum Complex Formation. The reaction of $[Pt(p\text{-}MeC_6H_4)(ppy)(SMe_2)]$, **1b**, with 0.5 equiv of dppf to form the binuclear complex $[Pt_2(p\text{-}MeC_6H_4)_2(ppy)_2(\mu\text{-}dppf)]$, **2b**, was monitored using variable-temperature ^{31}P NMR spectroscopy (202 MHz, in the range of 233−298 K), as shown in Figure 2.

Scheme 3

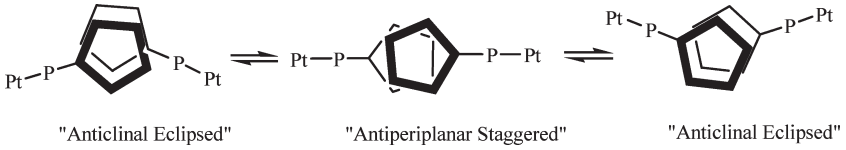

Scheme 4

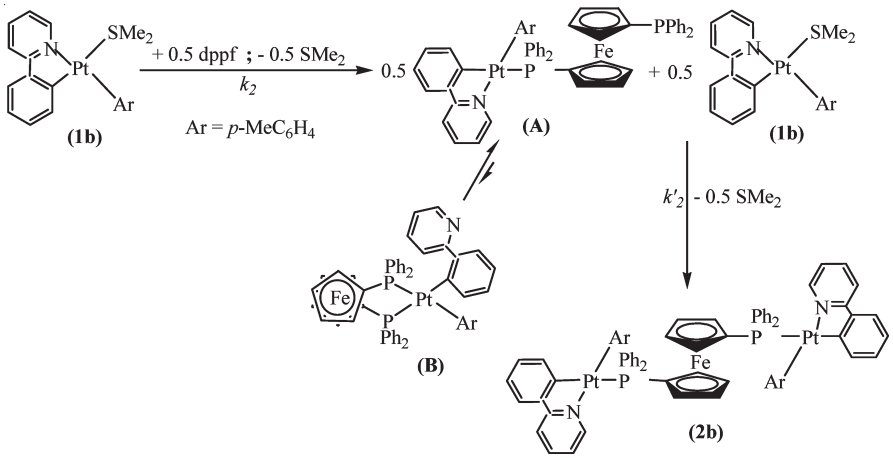

On the basis of the data obtained from the spectra, a mechanism described in Scheme 4 is suggested to occur during the reaction progress. Thus, **1b**, containing a labile SMe_2 ligand, is first attacked by dppf to form the intermediate complex [Pt(*p*-MeC_6H_4)(ppy)(dppf-κ^1P)], **A**, in which dppf-κ^1P is a monodentate dppf ligand;[6] 0.5 equiv of the starting complex **1b** remains unreacted. The formation of **A** is confirmed by the observation of a singlet signal at $\delta = -18.9$ ppm in the spectrum obtained at 233 K, due to the dangling phosphorus atom of the dppf ligand, and a rather broad singlet signal at δ = 12.4 ppm, which is coupled by the platinum center to give a $^1J_{PtP}$ value of 1842 Hz, due to the phosphorus atom of the dppf connected to platinum. The complex **A** is in equilibrium with the intermediate isomer complex [Pt(*p*-MeC_6H_4)(dppf)(ppy-κ^1C)], **B**, in which ppy-κ^1C is the deprotonated ppy ligand that is only C-ligated with the dangling N atom. During this dynamic process, the dangling dppf in complex **A** is converted to the chelating dppf, and as a result, the chelating C−N ligand is forced to open up from the N site. Note that we have previously indicated that when the Me analogue of **1b**, i.e., [PtMe(ppy)(SMe_2)], reacted with 1 mol of dppf, only the dppf chelate analogue complex [PtMe(dppf)(ppy-κ^1C)] was separated.[3a] However in the Ar analogue complexes **1** studied in the present work, the electron-withdrawing ability of Ar ligands is greater than that of the Me ligand, which favors the connection of the N ligating atom. More importantly, the fact that coordination around the dppf chelating **B** seems to be more sterically hindered than that of the dppf dangling analogue complex **A** is probably responsible for the formation of both **A** and **B** in equilibrium with each other. This has been confirmed with further theoretical studies (see next paragraph). The complex **A** is then slowly reacted with the remaining second half of the starting complex **1b** to give the final Pt(II)−Pt(II) binuclear complex [Pt_2(*p*-MeC_6H_4)$_2$(ppy)$_2$(μ-dppf)], **2b**. Consistently we found that if in a similar reaction less than 0.5 equiv of dppf is added, complex **2b** is formed accompanied by some unreacted starting complex **1b**. For **B** two signals appeared at δ 12.3 and 14.1 both with $^1J_{PtP}$ values almost equal to 1845 Hz, which is consistent with the *trans* influence of the *p*-MeC_6H_4 aryl ligand being almost equal to that of the ppy-κ^1C aryl ligand.[7] In our previous report of the ^{31}P NMR spectrum of the analogous dppf chelating complex [PtMe(dppf)(ppy-κ^1C)],[3a] the two related signals, appearing at δ = 20.5 and 23.9 ppm, indicated different $^1J_{PtP}$ values of 1995 and 1888 Hz due to the *trans* influence of Me ligand being higher than that of the ppy-κ^1C ligand. Overall, therefore, upon addition of dppf to the solution of **1b** (contributing no phosphorus signal), **A** is formed in an equilibrium with **B**. As time passes and the temperature is raised, **A** is consumed by **1b** and the final diplatinum complex **2b** is formed.

A series of calculations have been performed in order to investigate the relative stabilities of the isomers **A** and **B** (Schemes 4 and 5) as a function of the R ligand, in which R = Me, C≡CH, CF_3, H, or Ph. The lowest energy structures of the complexes [PtR(κ^2-*C*,*N*-ppy)(κ^1-*P*-dmpf)] (isomer **A**) and [PtR(κ^1-*C*-ppy)(κ^2-dmpf)] (isomer **B**) [dmpf = 1,1′-bis(dimethylphosphino)ferrocene], as calculated by density functional theory (DFT), are shown in Figure 3.[8]

Thus, when R = Me, C≡CH, CF_3, or H, the calculated energies for isomer **A** are 15.05, 13.15, 17.79, and 9.39 kJ mol^{-1}, respectively, greater than those calculated for isomer **B**. The results comply well with a greater preference for the κ^1-*C*-isomer **A** over isomer **B** for the case where R = Me as discussed above. Also, consistent with related geometrical isomerization discussed above for the **A** and **B** intermediates where R = Ph, the corresponding energies calculated for both isomers are almost equal. Although platinum(II) is a soft metal center that normally favors

dx.doi.org/10.1021/om101055n |*Organometallics* 2011, 30, 1466–1477

Scheme 5

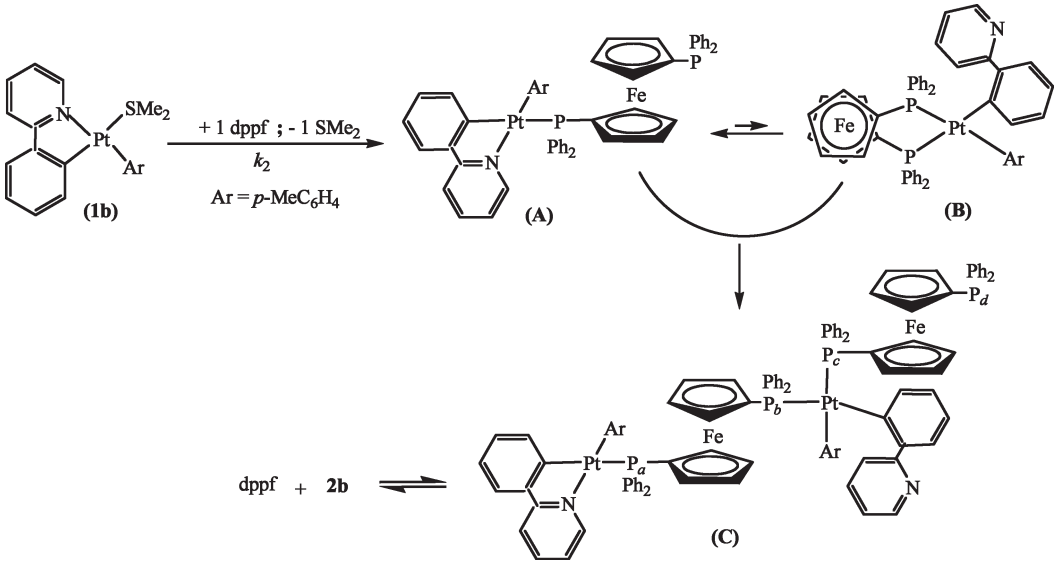

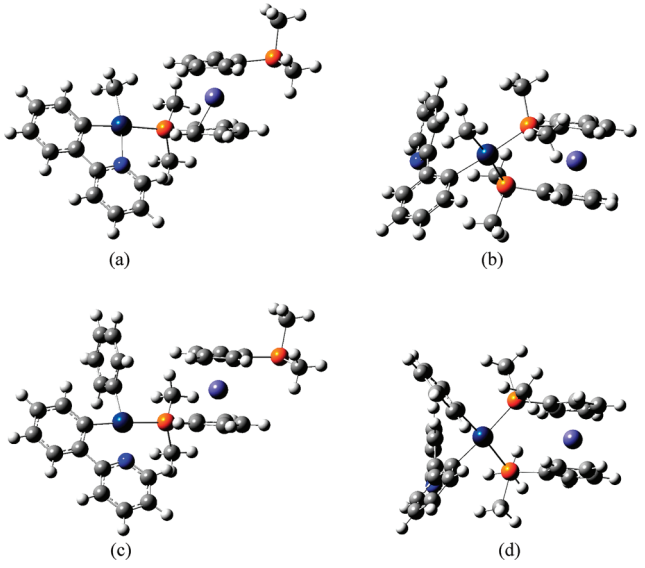

Figure 3. DFT-calculated structures of (a) [PtMe(κ^2-*C*,*N*-ppy)(κ^1-*P*-dmpf)] (isomer **A**), (b) [PtMe(κ^1-*C*-ppy)(κ^2-dmpf)] (isomer **B**), (c) [PtPh(κ^2-*C*,*N*-ppy)(κ^1-*P*-dmpf)] (isomer **A**), and (d) [PtPh(κ^1-*C*-ppy)(κ^2-dmpf)] (isomer **B**).

phosphorus over nitrogen coordination, the electron-withdrawing ability of the Ar ligand and more importantly its steric hindrance favor an equilibrium between **A** and **B** for the case in which R = Ph.

Reaction of 1b with 1 equiv of dppf. The results obtained from reaction of **1b** with 1 equiv of dppf are described in Scheme 5. On the basis of the ^{31}P and ^{195}Pt NMR spectra we suggest that upon the addition of dppf at room temperature (see Figure 4), complex **1b** is completely converted to the dangling complex **A**, via displacement of the SMe_2 labile ligand. As was mentioned above for the related reaction involving addition of 0.5 equiv of dppf (see Scheme 4 and the above related theoretical discussion), **A** is in equilibrium with the chelate analogous **B**. The two complexes **A** and **B** then are reacted with each other to form complex **C**, during which the P dangling atom in **A** attacks the Pt center of **B** to open up the chelating dppf. Complex **C** finally dissociates and forms an equilibrium with the dimeric complex **2b** by releasing free dppf. Similar results are observed when more than 1 equiv of dppf (e.g., 2 equiv) is used in the related reaction, except for slight variations in the ratio of the product components, **2b**:**C**:free-dppf. The assignments for the complexes are indicated in Figure 4. The sharp singlet signal observed at δ = 20.6 (with $^1J_{PtP}$ = 2004 Hz) is due to the bridged complex **2b** with the related free dppf appearing at δ = −17.3. The sharp signal appearing at δ = 20.9 (with $^1J_{PtP}$ = 2014 Hz) has almost the same parameters as those for the rather broad signal of **2b**, and we therefore attribute it to P_a of the suggested product **C** with the doublets at δ = 15.5 ($^2J_{PbPc}$ = 15 Hz and $^1J_{PtP}$ = 1895 Hz) and δ = 12.2 ($^1J_{PtP}$ = 1845 Hz and $^2J_{PbPc}$ = 15 Hz) being assigned to its P_c and P_b, respectively, and the signal at δ = −17.8 to its dangling phosphorus atom P_d. In the corresponding ^{195}Pt NMR spectrum, the broad doublet signal at δ = −2410 (with $^1J_{PtP}$ = 1990 Hz) is assigned to the two overlapped Pt signals of **2b** and **C**, and a broad triplet at δ = −2820 with $^1J_{PtP}$ = 1890 Hz is assigned to the second Pt atom of complex **C** (see Figure 4).

In order to confirm the last step of the reaction, i.e., dissociation of **C** to form an equilibrium with **2b** and free dppf (see Scheme 5), a pure sample of **2b** was reacted with 1 (or even 2) equiv of dppf, and on the basis of the ^{31}P NMR spectrum we found that complex **C** was formed as a mixture with **2b** and free dppf. In addition, attempts were also made to extend the length of the chain in complex **C** from the terminal dangling P atom by using other complexes bearing labile ligands, but fragmentation of the type described in Scheme 6 may have taken place. Thus, when a solution of the mixture {**C** + **2b** + dppf}, obtained from the reaction of **1b** with 1 equiv of dppf (as described above), was reacted with [PtR(ppy)(SMe_2)], in which R = Ph or Me (equivalent amount being calculated approximately as twice the amount of the components **C** and free dppf in the starting mixture), we found that in each case a mixture containing mainly unreacted **2b** and an unsymmetrical complex, [(p-MeC_6H_4)(ppy)Pt-(μ-dppf)PtR(ppy)] (R = Ph, **3a**, or R = Me, **3b**), was obtained.

dx.doi.org/10.1021/om101055n |*Organometallics* 2011, 30, 1466–1477

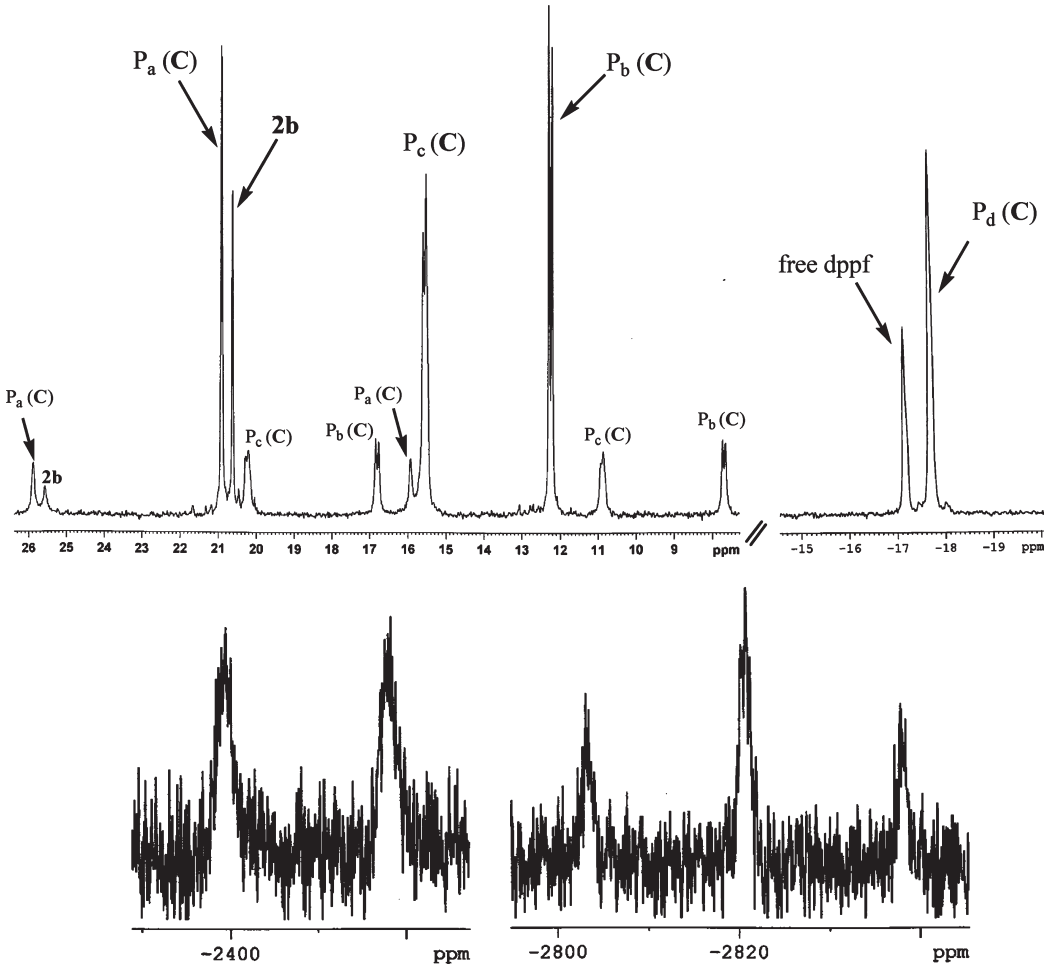

Figure 4. ^{31}P (top view) and ^{195}Pt (bottom view) NMR spectra obtained after addition of 1 equiv of dppf to a solution of the complex [Pt(*p*-MeC_6H_4)(ppy)(SMe_2)], **1b**, at room temperature.

It is probable that at first complex **C** assembles with [PtR(ppy)(SMe_2)] to form **X**, but this triplatinum(II) complex is then fragmented to the unsymmetrical complex **3** and the dangling dppf complex **A**. The latter further reacts with [PtR(ppy)(SMe_2)] to obtain **3**; as expected, when R = *p*-MeC_6H_4, then **2b** is the main product (see Scheme 6).

Kinetic Studies. *Addition of 0.5 equiv of dppf.* In this case, we found that the species involved in the reaction (reactants, products, and intermediates) have overlapped spectra, and so the rate constant determination by conventional curve-fitting methods is not feasible. However, by using chemometric methods, as an emerging computational tool in chemistry, we have been able to study the complex kinetic systems involved in this process having severe spectral overlapping. In addition, they can give information about the number of chemical components coexisting in a reaction, which is useful in mechanistic studies.

The above-mentioned mechanism of the dimer complex formation was further studied by the spectrophotometric kinetics of the initial addition of 0.5 equiv of dppf in dichloromethane. The change in the absorbance spectra of the reaction mixture during a typical kinetic run is shown in Figure 5. Preliminary results show that when dppf is added to **1b** in solution, the absorbance decreases quickly in the region 330−700 nm in the first 30 min, and after that the absorbance slightly increases along with time. The change of absorbance at 360 nm as a function of time is plotted as the inset in Figure 5. These results show that the reaction mechanism of addition of dppf to **1b** may be considered as a competitive-consecutive second-order process of the form of eq 1:

$$\begin{aligned} \mathbf{1b} + \text{dppf} &\xrightarrow{k_2} \mathbf{A} \\ \mathbf{A} + \mathbf{1b} &\xrightarrow{k_2'} \mathbf{2b} \end{aligned} \qquad (1)$$

Differentiation of the **A** and **B** intermediate species seems to be difficult by using the data obtained from the UV−visible spectroscopy, as the species have very similar spectra. From the chemometrics point of view, the kinetic system of eq 1 is denoted as rank deficient since changes in the concentration of one component as function of time can be written as a linear function of the other species. Thus, in spite of having four chemical components, they can be described by three noncorrelated orthogonal linear combinations. The proposed mechanism for reaction was confirmed by principal component analysis (PCA).[9] The main aim of PCA is to determine the number of principal components, and the obtained results indicate the numbers of independent systematic variations in the spectral data. It was found (see score plots in Figure S1(a) in the Supporting Information) that the recorded absorbance data matrix can be best explained by three significant principal components (PCs). This implies that the

dx.doi.org/10.1021/om101055n |*Organometallics* 2011, 30, 1466–1477

Scheme 6

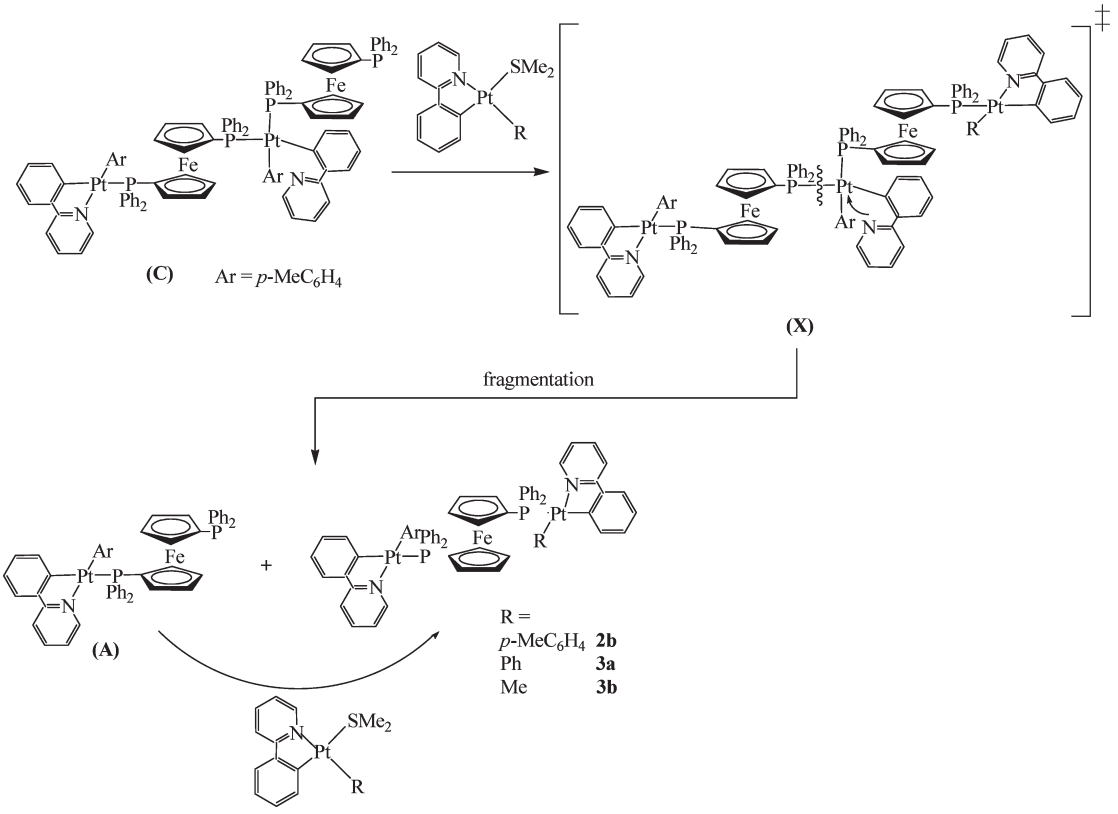

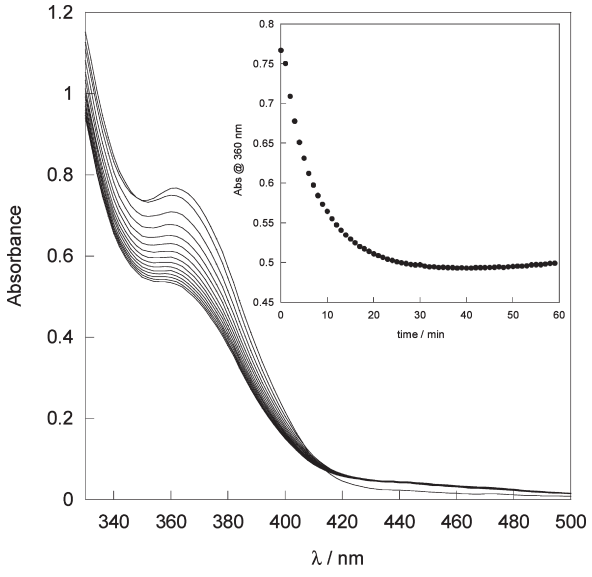

Figure 5. Change in the absorbance spectra of complex **1b** upon addition of 0.5 equiv of dppf as function of time. Inset is the variation of absorbance at 360 nm over time.

process is rank deficient, and the considered second-order consecutive reaction mechanism may well be correct.

Chemometrics resolution of the rank-deficient chemical system is a difficult task, and the methods that are able to resolve such systems have high scientific impacts. To overcome and break the rank deficiency, a column-wise data matrix augmentation was used.[10] To do so, the absorbance spectra of **1b** without addition of dppf were recorded in the same time interval as in the presence of dppf, and a new data matrix was obtained. Thus, the augmented data matrix is composed of the changes in absorbance spectra of **1b** as a function of time in the presence and absence of dppf. The number of rows of this matrix is 2 times each individual matrix, whereas the number of columns is equal to each individual one. As it is shown (see the score plots of Figure S1(b) in the Supporting Information), the augmented data matrix is explained by four factors, and we see that rank deficiency is broken. The augmented data matrix is now full rank. It should be noted that augmentation of the reaction mixture data matrix with the absorbance data matrix of **1b** alone does not add a new chemical factor since **1b** is presented in both data matrices. Thus data augmentation unraveled one of the hidden chemical factors.

Once the problem of rank deficiency was overcome, a hard-modeling-based multivariate curve resolution (MCR) technique was employed for determination of kinetic constants and resolution of the pure spectra of the components involved in the reaction.[11] This algorithm is explained briefly in the Supporting Information.

The estimated rate constants for three repeated batch processes by applying the proposed method are $k_2 = 10.7 \pm 0.2$ L mol^{-1} s^{-1} and $k_2' = 0.68 \pm 0.05$ L mol^{-1} s^{-1}. The concentration and spectral profiles of the reactants and products calculated based on the average rate constants are shown in Figure 6. A high degree of similarity between the resolved pure spectra of dppf and complex **1b** and their experimental spectra was obtained. This confirms the accuracy of the results obtained by the employed chemometric methods. In addition to estimating the

dx.doi.org/10.1021/om101055n |*Organometallics* 2011, 30, 1466–1477

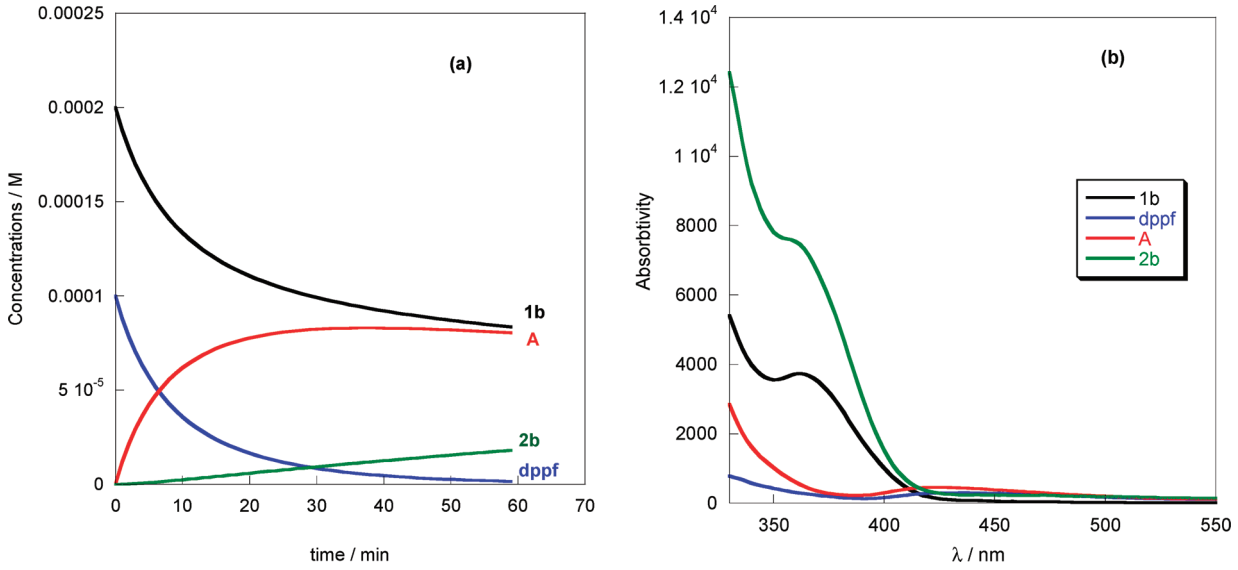

Figure 6. Resolved concentration profiles (a) and pure spectra (b) of the species coexisting in the studied reaction.

rate constants of such complex systems by spectrophotometric method, another advantage of the MCR method is estimating the pure spectra of intermediate species **A**, which cannot be recorded experimentally.

Addition of 1 equiv of dppf. The reaction of **1b** with 1 equiv of dppf was monitored by the more conventional UV−visible spectrophotometric techniques, and the data were obtained under second-order conditions ($[\text{dppf}]_0 = [\mathbf{1b}]_0$). The data were fitted to eq 2 with the programs that are based on the least-squares method.

$$\text{Abs}_t = \text{Abs}_\infty + (\text{Abs}_0 - \text{Abs}_\infty)/(1 + [\mathbf{1b}]_0 \times k_2 \times t) \quad (2)$$

The k_2 value was evaluated by nonlinear least-squares fitting of the absorbance−time profiles to eq 2. The same method was used at different temperatures, and activation parameters were obtained from the Eyring equation (eq 3 and Figure 7). The results are collected in Table 1. It is interesting to note that the value $k_2 = 10.5 \pm 0.5$ L mol^{-1} s^{-1} at 5 °C, which is related to the first step of the reaction, is in excellent agreement with the value obtained from the chemometric method at a concentration ratio of [dppf]/[**1b**] = 0.5:1 for the first step of the reaction.

$$\ln\left(\frac{k_2}{T}\right) = \ln\left(\frac{k_B}{h}\right) + \frac{\Delta S^{\ddagger}}{R} - \frac{\Delta H^{\ddagger}}{RT} \quad (3)$$

Addition of Excess dppf. The addition reaction of dppf to **1b** ($[\text{dppf}]_0 \gg [\mathbf{1b}]_0$) in CH_2Cl_2 at 5 °C was studied using UV−visible spectroscopy. In each case, excess dppf at different concentrations was used, and the change in absorbance was monitored. The reaction followed good first-order kinetics. The pseudo-first-order rate constants (k_{obs}) were evaluated by nonlinear least-squares fitting of the absorbance−time profiles to a first-order equation (eq 4):

$$\text{Abs}_t = \text{Abs}_\infty + (\text{Abs}_0 - \text{Abs}_\infty)\exp(-k_{obs}t) \quad (4)$$

A Graph of these pseudo-first-order rate constants against the concentration of dppf gave a good straight line plot passing through the origin, showing a first-order dependence of the rate on the concentration of dppf (Figure 8), and the slope gave an overall

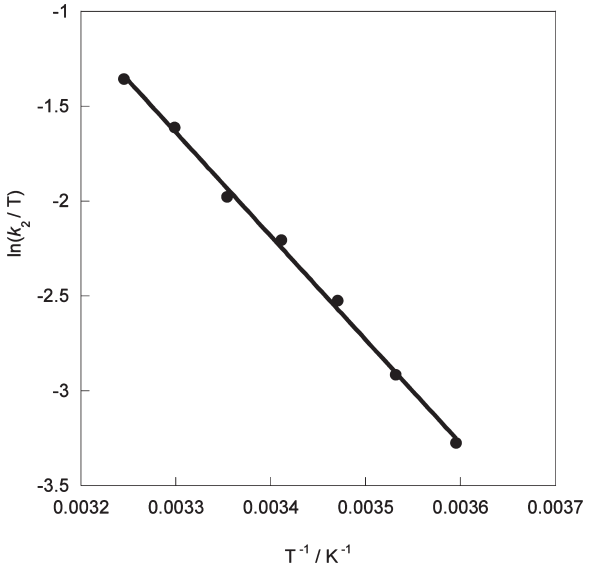

Figure 7. Eyring plot for the reaction of **1b** with dppf in CH_2Cl_2.

second-order rate constant. The rate constant was obtained as $k_2 = 10.6 \pm 0.6$ L mol^{-1} s^{-1}, in agreement with values obtained for the 0.5:1 and 1:1 ratio cases described above. Note that the reaction of dppf with **1b** under pseudo-first-order conditions was too fast to be measured at higher temperatures.

Electroluminescence Properties of Complexes 1b and 2b. Single-layer OLEDs were fabricated on glass substrates that had beforehand been precleaned by ultrasonic treatment in detergent, deionized water, acetone, and methanol, respectively, and pretreated with oxygen plasma cleaner before use. These layers were then precoated with a layer of indium tin oxide (ITO). Organic layers and cathode layers (Al) were deposited by conventional vacuum vapor deposition below 2×10^{-6} Torr. The thickness of each layer was determined by a quartz thickness monitor. The effective size of the light-emitting diode was 9 mm^2. The absorption and electroluminescence (EL) spectra were measured under ambient conditions at room temperature. The

dx.doi.org/10.1021/om101055n |*Organometallics* 2011, 30, 1466–1477

Table 1. Rate Constants[a] and Activation Parameters for the Reaction of 1b with dppf in CH_2Cl_2

	T = 5 °C	T = 10 °C	T = 15 °C	T = 20 °C	T = 25 °C	T = 30 °C	T = 35 °C	$\Delta H^{\ddagger}$/kJ mol^{-1}	$\Delta S^{\ddagger}$/J K^{-1} mol^{-1}
k_2 (L mol^{-1} s^{-1})	10.5	15.3	23.1	32.3	41.3	60.5	79.4	45.4 ± 1.0	−61 ± 4

[a] Estimated errors in k_2 values are ±4%.

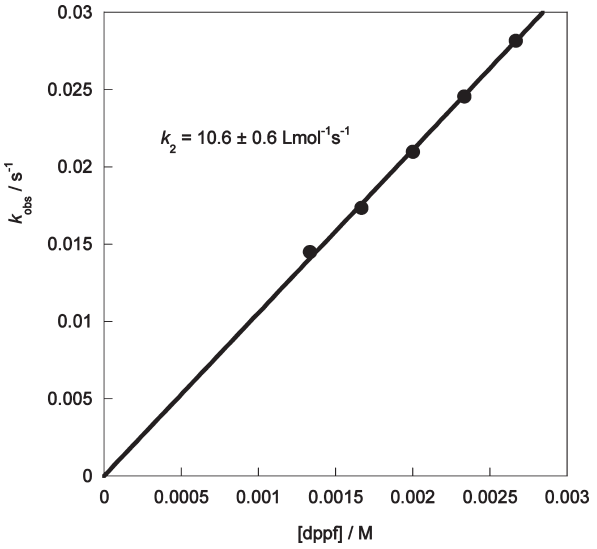

Figure 8. Plot of first-order rate constants (k_{obs}/s^{-1}) for the reaction of **1b** (2×10^{-4} M) with dppf in CH_2Cl_2 at T = 5 °C vs concentration of dppf.

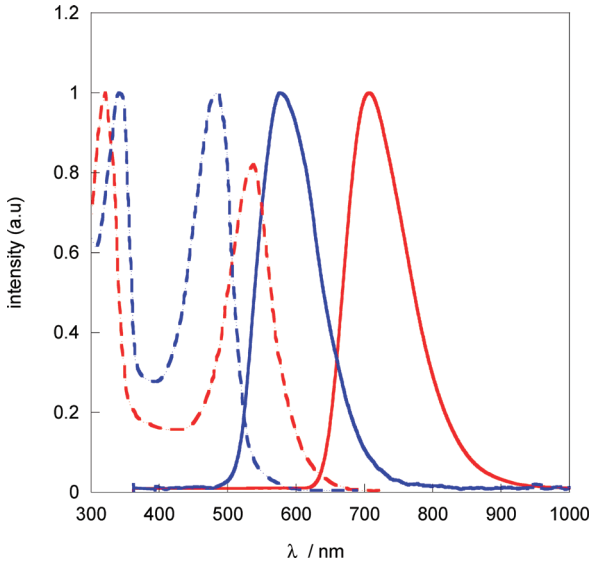

Figure 9. Absorption (dashed lines) and photoluminescence spectra (solid lines) of **1b** (blue) and **2b** (red).

absorption spectra were measured using a Perkin-Elmer Lambda 25 UV−vis spectrometer. The EL spectra were recorded using a Si detector that is calibrated up to 900 nm and is thus suitable for recording only the visible EL spectra.

Figure 9 shows a comparison between the absorption and EL spectra of the two complexes **1b** and **2b**. Thus, while both complexes show strong absorptions at λ = 320 to 345 nm, **1b** has a longer wavelength absorption peak at λ = 485 nm, which is significantly red-shifted to λ = 637 nm for **2b**. This is consistent with the lower HOMO−LUMO energy gap in the latter complex. Correspondingly, the EL of compound **2b**, peaked at λ = 710 nm, is also significantly red-shifted as compared to that of **1b**, having a peak at λ = 580 nm.

EXPERIMENTAL SECTION

The ^{1}H NMR spectra were recorded on a Bruker Avance DPX 250 MHz spectrometer, and the ^{31}P and ^{195}Pt NMR spectra were recorded on a Bruker Avance DRX 500 MHz spectrometer. The operating frequencies and references, respectively, are shown in parentheses as follows: ^{1}H (250 MHz, TMS), ^{31}P (202 MHz, 85% H_3PO_4), and ^{195}Pt (107 MHz, aqueous Na_2PtCl_4). The chemical shifts and coupling constants are in ppm and Hz, respectively. The microanalyses were performed using a Thermofinnigan Flash EA-1112 CHNSO rapid elemental analyzer. Kinetic studies were carried out by using a Perkin-Elmer Lambda 25 spectrophotometer with temperature control using an EYELA NCB-3100 constant-temperature bath. 2-Phenylpyridine, benzo[*h*]quinoline, and 1,1′-bis(diphenylphosphino)ferrocene were purchased from Aldrich, and *cis*-[$PtAr_2(SMe_2)_2$] (Ar = Ph, *p*-MeC_6H_4, and *p*-$MeOC_6H_4$), [Pt(*p*-MeC_6H_4)(ppy)(SMe_2)], **1b**, [Pt(*p*-MeC_6H_4)(bhq)(SMe_2)], **1b′**, [Pt(*p*-$MeOC_6H_4$)(ppy)(SMe_2)], **1c**, and [Pt(*p*-$MeOC_6H_4$)(bhq)(SMe_2)], **1c′**, have been prepared by the known methods.[12a−d]

[Pt(C_6H_5)(C−N)(SMe_2)], 1a or 1a′. To a solution of *cis*-[Pt-(C_6H_5)$_2$(SMe_2)$_2$] (200 mg, 0.42 mmol) in acetone (30 mL) was added 2-phenylpyridine (61.3 μL, 0.42 mmol for **1a**) or benzo[*h*]quinoline (75.8 mg, 0.42 mmol for **1a′**), and the reaction mixture was refluxed for 4 h. A light green solution was formed; then the solvent was removed under reduced pressure and the residue was triturated with cold acetone (2 × 2 mL). The products as a light green solid were dried under vacuum. **1a**: Yield: 125 mg; 61%, mp 216 °C (dec). Anal. Calcd for $C_{19}H_{19}NPtS$: C, 46.7; H, 3.9; N, 2.9. Found: C, 46.7; H, 3.8; N, 2.8. ^{1}H NMR data in $CDCl_3$: δ 2.20 (s, $^3J_{PtH}$ = 25.5 Hz, Me groups of SMe_2 ligand, 6H), (aromatic protons): 7.59 (d, $^3J_{PtH^o}$ = 57.5 Hz, $^3J_{H^oH^m}$ = 6.7 Hz, H^o of phenyl ligand, 2 H^o), 8.86 (d, $^3J_{PtH^6}$ = 18.8 Hz, $^3J_{H^6H^5}$ = 5.1 Hz, H^6 of ppy ligand, 1 H^6), other aromatic protons of phenyl and ppy ligands: 6.80−8.00, 10 H. **1a′**: Yield: 162 mg; 75%, mp 206 °C (dec). Anal. Calcd for $C_{21}H_{19}NPtS$: C, 49.2; H, 3.7; N, 2.7. Found: C, 49.4; H, 3.6; N, 2.7. ^{1}H NMR data in $CDCl_3$: δ 2.28 (s, $^3J_{PtH}$ = 26.3 Hz, Me groups of SMe_2 ligand, 6H), (aromatic protons): 9.13 (d, $^3J_{PtH^6}$ = 18.1 Hz, $^3J_{H^6H^5}$ = 5.0 Hz, H^6 of bhq ligand, 1 H^6), other aromatic protons of phenyl and bhq ligands: 7.00−8.34, 12 H.

[$Pt_2(C_6H_5)_2(ppy)_2(\mu$-dppf)], 2a. To a solution of **1a** (196 mg, 0.40 mmol) in acetone (30 mL) was added 0.5 equiv of dppf (113.6 mg, 0.20 mmol), and the solution was stirred for 2 h. A yellow solution was formed; then the solvent was removed under reduced pressure and the residue was triturated with cold acetone (2 × 3 mL). The product as a yellow solid was dried under vacuum. Yield: 82%, mp 266 °C (dec). Anal. Calcd for $C_{68}H_{54}FeN_2P_2Pt_2$: C, 58.0; H, 3.9; N, 2.0. Found: C, 57.9; H, 3.8; N, 1.9. NMR data in $CDCl_3$: ^{1}H NMR: δ 3.35 (br s, β, β' Cp protons, 4 H), 4.31 (br s, α, α' Cp protons, 4 H), (aromatic protons): 7.34 (d, $^3J_{H^oH^m}$ = 6.4 Hz, H^o of phenyl ligand, 4 H^o), 7.76 (d, $^3J_{PtH^6}$ = 18.5 Hz, $^3J_{H^6H^5}$ = 8.1 Hz, H^6 of ppy ligand, 2 H^6), other aromatic protons of phenyl, ppy, and dppf ligands: 6.50−8.00, 40 H. ^{31}P NMR: δ 21.0 (s, $^1J_{PtP}$ = 2006 Hz, 2 P). ^{195}Pt NMR: δ −2407 (d, $^1J_{PtP}$ = 2000 Hz, 2 Pt).

The following complexes were made similarly using the appropriate starting precursors.

dx.doi.org/10.1021/om101055n |*Organometallics* 2011, 30, 1466–1477

[$Pt_2(C_6H_5)_2(bhq)_2(\mu$-dppf)], 2a′. This was prepared similarly using **1a′** (200 mg, 0.39 mmol) and dppf (105.3 mg, 0.19 mmol) in acetone (30 mL). Yield: 197 mg, 64%, mp 225 °C (dec). Anal. Calcd for $C_{72}H_{54}FeN_2P_2Pt_2$: C, 59.4; H, 3.7; N, 1.9. Found: C, 59.6; H, 3.8; N, 2.0. NMR data in $CDCl_3$: ^{1}H NMR: δ 3.40 (br s, β, β' Cp protons, 4 H), 4.41 (br s, α, α' Cp protons, 4 H), (aromatic protons): 8.12 (d, $^3J_{PtH^6}$ = 18.4 Hz, $^3J_{H^6H^5}$ = 7.9 Hz, H^6 of bhq ligand, 2 H^6), other aromatic protons of aryl, bhq, and dppf ligands: 6.85−7.95, 44 H. ^{31}P NMR: δ 20.5 (s, $^1J_{PtP}$ = 2069 Hz, 2 P). ^{195}Pt NMR: δ −2433 (d, $^1J_{PtP}$ = 2051 Hz, 2 Pt).

[$Pt_2(p$-$MeC_6H_4)_2(ppy)_2(\mu$-dppf)], 2b. This was prepared similarly using **1b** (200 mg, 0.4 mmol) and dppf (113.6 mg, 0.2 mmol) in acetone (30 mL). Yield: 190 mg, 61%, mp 223 °C (dec). Anal. Calcd for $C_{70}H_{58}FeN_2P_2Pt_2$: C, 58.6; H, 4.1; N, 1.9. Found: C, 57.9; H, 4.4; N, 1.8. NMR data in $CDCl_3$: ^{1}H NMR: δ 2.17 (s, Me groups on the *p*-tolyl ligands, 6H), 3.39 (br s, β, β' Cp protons, 4 H), 4.37 (br s, α, α' Cp protons, 4 H), (aromatic protons): 6.57 (d, $^3J_{H^mH^o}$ = 7.2 Hz, H^m of *p*-tolyl ligand, 4 H^m), 7.08 (d, $^3J_{PtH^o}$ = 65.5 Hz, $^3J_{H^oH^m}$ = 6.8 Hz, H^o of *p*-tolyl ligand, 4 H^o), 7.76 (d, $^3J_{PtH^6}$ = 18.3 Hz, $^3J_{H^6H^5}$ = 7.8 Hz, H^6 of ppy ligand, 2 H^6), other aromatic protons of aryl, and dppf ligands: 6.45−7.80, 34 H. ^{31}P NMR: δ 20.6 (s, $^1J_{PtP}$ = 2004 Hz, 2 P). ^{195}Pt NMR: δ −2409 (d, $^1J_{PtP}$ = 1990 Hz, 2 Pt).

[$Pt_2(p$-$MeC_6H_4)_2(bhq)_2(\mu$-dppf)], 2b′. This was prepared similarly using **1b′** (200 mg, 0.38 mmol) and dppf (105.3 mg, 0.19 mmol) in acetone (30 mL). Yield: 208 mg, 68%, mp 270 °C (dec). Anal. Calcd for $C_{74}H_{58}FeN_2P_2Pt_2$: C, 59.9; H, 3.9; N, 1.9. Found: C, 59.6; H, 3.9; N, 2.0. NMR data in $CDCl_3$: ^{1}H NMR: δ 2.09 (s, Me groups on the *p*-tolyl ligands, 6H), 3.44 (br s, β, β' Cp protons, 4 H), 4.47 (br s, α, α' Cp protons, 4 H), (aromatic protons): 6.61 (d, $^3J_{H^mH^o}$ = 7.7 Hz, H^m of *p*-tolyl ligand, 4 H^m), 8.12 (d, $^3J_{PtH^6}$ = 18.7 Hz, $^3J_{H^6H^5}$ = 8.1 Hz, H^6 of bhq ligand, 2 H^6), other aromatic protons of aryl, bhq, and dppf ligands: 6.75−7.90, 38 H. ^{31}P NMR: δ 20.0 (s, $^1J_{PtP}$ = 2067 Hz, 2 P). ^{195}Pt NMR: δ −2435 (d, $^1J_{PtP}$ = 2118 Hz, 2 Pt).

[$Pt_2(p$-$MeOC_6H_4)_2(ppy)_2(\mu$-dppf)], 2c. This was prepared similarly using **1c** (200 mg, 0.39 mmol) and dppf (105.3 mg, 0.19 mmol) in acetone (30 mL). Yield: 202 mg, 66%, mp 208 °C (dec). Anal. Calcd for $C_{70}H_{58}FeN_2O_2P_2Pt_2$: C, 57.3; H, 4.0; N, 1.9. Found: C, 57.2; H, 3.8; N, 2.1. NMR data in $CDCl_3$: ^{1}H NMR: δ 3.77 (s, OMe groups on the *p*-anisyl ligands, 6H), 3.42 (br s, β, β' Cp protons, 4 H), 4.32 (br s, α, α' Cp protons, 4 H), (aromatic protons): 6.42 (d, $^3J_{H^mH^o}$ = 8.2 Hz, H^m of *p*-anisyl ligand, 4 H^m), 7.76 (d, $^3J_{PtH^6}$ = 18.2 Hz, $^3J_{H^6H^5}$ = 7.9 Hz, H^6 of ppy ligand, 2 H^6), other aromatic protons of aryl, ppy, and dppf ligands: 6.35−7.90, 38 H. ^{31}P NMR: δ 20.8 (s, $^1J_{PtP}$ = 1992 Hz, 2 P). ^{195}Pt NMR: δ −2405 (d, $^1J_{PtP}$ = 1980 Hz, 2 Pt).

[$Pt_2(p$-$MeOC_6H_4)_2(bhq)_2(\mu$-dppf)], 2c′. This was prepared similarly using **1c′** (200 mg, 0.36 mmol) and dppf (102.1 mg, 0.18 mmol) in acetone (30 mL). Yield: 196 mg, 65%, mp 267 °C (dec). Anal. Calcd for $C_{74}H_{58}FeN_2O_2P_2Pt_2$: C, 58.6; H, 3.9; N, 1.8. Found: C, 58.5; H, 3.8; N, 1.8. NMR data in $CDCl_3$: ^{1}H NMR: δ 3.71 (s, OMe groups on the *p*-anisyl ligands, 6H), 3.42 (br s, β, β' Cp protons, 4 H), 4.42 (br s, α, α' Cp protons, 4 H), (aromatic protons): 6.48 (d, $^3J_{H^mH^o}$ = 8.5 Hz, H^m of *p*-anisyl ligand, 2 H^m), 8.12 (d, $^3J_{PtH}{}^6$ = 19.0 Hz, $^3J_{H^6H^5}$ = 8.1 Hz, H^6 of bhq ligand, 1 H^6), other aromatic protons of aryl, bhq, and dppf ligands: 6.70−8.00, 38 H. ^{31}P NMR: δ 20.2 (s, $^1J_{PtP}$ = 2055, 2 P). ^{195}Pt NMR: δ −2432 (d, $^1J_{PtP}$ = 1979, 2 Pt).

[(p-MeC_6H_4)(ppy)Pt(μ-dppf)Pt(p-MeC_6H_4)(ppy-κ^1C)(dppf-κ^1P)], C. In the above procedure, used to prepare **2b**, when **1b** (200 mg, 0.4 mmol) was reacted with 1 equiv of dppf (227.2 mg, 0.4 mmol), complex **C** was obtained as a mixture with **2b** and dppf, and the components of the mixture were not isolable. NMR data for complex **C** in $CDCl_3$: ^{1}H NMR: δ 2.18 and 2.20 (s, Me groups on the *p*-tolyl ligands, 6 H), 3.49−4.80 (Cp protons, 16 H), (aromatic protons): 6.14−8.18 (aromatic protons of *p*-tolyl, ppy, and dppf ligands, 80 H). ^{31}P NMR: δ 20.9 (s, $^1J_{PtP}$ = 2014, P_a, 1 P), 15.5 (d, $^1J_{PtP}$ = 1895, $^2J_{PbPc}$ = 15, P_c, 1 P), 12.2 (d, $^1J_{PtP}$ = 1845, $^2J_{PbPc}$ = 15, P_b, 1 P), −17.8 (s, P_d, 1 P). ^{195}Pt NMR: δ −2409 (d, $^1J_{PtP}$ = 1994 Hz, Pt_a), −2821 (t, $^1J_{PtP}$ = 1891 Hz, Pt_b).

Table 2. Crystal Data and Data Collection and Structure Refinement Details for the Complex [$Pt_2(p$-$MeOC_6H_4)_2(bhq)_2(\mu$-dppf)], 2c′·CH_2Cl_2

formula	$C_{75}H_{60}Cl_2FeN_2O_2P_2Pt_2$
fw	1685.10
cryst syst	monoclinic
space group	*C*2/*c*
a/Å	12.540(3)
b/Å	14.801(3)
c/Å	32.631(7)
β/deg	95.88(3)°
vol/Å^3	6025(2)
Z	4
D(calc)/Mg m^{-3}	1.764
abs coeff/mm^{-1}	5.064
F(000)	3144
no. of collected reflns	22 925
no. of independent reflns	9151 [*R*(int) = 0.086]
no. of obsd reflns [$I > 2\sigma(I)$]	6688
data/restraints/params	9151/0/387
T_{min}/T_{max}	0.4161/0.5817
largest diff peak, hole [e Å^{-3}]	1.29 and −1.61
Goof (F^2)	1.056
R_1, wR_2 [$I > 2\sigma(I)$]	0.0590, 0.1369
R_1, wR_2 (all data)	0.0855, 0.1529

Monitoring the Reaction by ^{31}P NMR Spectroscopy. A small sample (10 mg) of **1b** was dissolved in $CDCl_3$ (0.75 mL) in an NMR tube, and either 0.5 or 1 equiv or excess dppf was added. Then the NMR spectra were recorded.

Kinetic Study. A 3.0 mL portion of a 2.0 × 10^{-4} M solution of **1b** was transferred into a thermostated quartz cell (path length: 10 mm), and a known volume of 0.01 M dppf was added using a microsyringe. The absorbance spectra of the reaction mixture were rapidly monitored with time.

X-ray Structure Determination. Single crystals of [$Pt_2(p$-$MeOC_6H_4)_2(bhq)_2(\mu$-dppf)], **2c′**·CH_2Cl_2, were grown from a concentrated CH_2Cl_2 solution by slow diffusion of *n*-hexane. A red-orange needle of approximate 0.21 × 0.16 × 0.12 mm in size was mounted on a glass fiber. All measurements were made on a STOE IPDSII diffractometer with a graphite monochromator using Mo Kα radiation. The data were collected at 298 K and integrated using the Stoe X-AREA[13] software package. Crystal data and data collection and structure refinement details are listed in Table 2. A numerical absorption correction was applied using the X-RED[14] and X-SHAPE[15] software programs. The data were corrected for Lorentz and polarization effects. No decay correction was applied. The structure was solved by direct methods.[16] All of the non-hydrogen atoms were refined anisotropically. All of the hydrogen atoms were positioned geometrically and refined with a riding model approximation with U_{iso}(H) = 1.2 or 1.5U_{eq}(C). Molecular graphics were performed using SHELXTL.[16] Crystallographic data for the structural analysis have been deposited with the Cambridge Crystallographic Data Center, CCDC no. 786085. Copies of this information may be obtained free of charge from the Director, CCDC, 12 Union Road, CB2 1EZ, U.K. (http://www.ccdc.cam.ac.uk).

DFT Calculations. Gaussian 09 was used[8] to fully optimize all the structures reported in this paper at the B3LYP[17] level of density

functional theory. The effective core potential of Hay and Wadt with a double-ξ valence basis set (LANL2DZ) was chosen to describe Pt.[18] The 6-31G(d) basis set was used for other atoms.[19] A polarization function of ξ_f = 1.472 was also added to Pt.[20] This basis set combination will be referred to as BS1. Frequency calculations were carried out at the same level of theory as for structural optimization. To further refine the energies obtained from the B3LYP/BS1 calculations, we carried out single-point energy calculations for all the structures with a larger basis set (BS2). BS2 utilizes the quadruple-ζ valence def2-QZVP[21] basis set on Pt along with the corresponding ECP and the 6-311+G(2d,p) basis set on other atoms. We have used the energies obtained from B3LYP/BS2//B3LYP/BS1 throughout the paper unless otherwise stated.

CONCLUSION

Although the complexes with monodentate dppf ligands are rare,[6a] and there is no example of such a mode of dppf ligand in platinum chemistry, we found that replacement of the labile ligand SMe_2 in the cyclometalated complex [Pt(*p*-MeC_6H_4)(ppy)(SMe_2)], **1b**, by dppf first gives the stable, uncommon complex [Pt(*p*-MeC_6H_4)(ppy)(dppf-κ^1P)], **A**, with a monodentate dppf ligand. Complex **A** is obtained (under **1b**:dppf = 1:0.5 ratio) in equilibrium with an isomeric form, [Pt(*p*-MeC_6H_4)(dppf)(ppy-κ^1C)], **B**. The intermediate complex **A** is then slowly reacted with the second half of starting complex **1b** to give the final Pt(II)−Pt(II) binuclear complex [Pt_2(*p*-MeC_6H_4)$_2$(ppy)$_2$(μ-dppf)], **2b**. In complex **B**, as compared to complex **A**, the great chelating appetite of dppf has caused the cyclometalated chelate to open up from the N donor atom. This indicates that opening of the rather strong cyclometalated ring from the N chelating atom has a rather comparable tendency to that of converting a chelating dppf ligand to an uncommon case of monodentate dppf ligand. Also, the chelating dppf ligand in organoplatinum(II) complexes has a PPtP bite angle usually close to 100°,[4,5] which is significantly greater than 90°, and this implies that the chelating dppf is also under strain. So as observed in the present study (see Scheme 4) and our previous one,[3] the chelating dppf and the chelating C−N ligands are sometimes competing with each other in "chelate opening".

When complex **2b**, with its "anticlinal eclipsed" conformation, is dissolved in solvent, a fluxionality of the type shown in Scheme 3 is suggested to occur so that on average the "antiperiplanar staggered" conformation, with an ideal torsion angle of 180°, is observed.

Kinetic study of formation of **2b** from the reaction of **1b** with dppf (1:0.5) is done, and a competitive-consecutive second-order reaction mechanism is proposed. The rate constants of the two steps were obtained using chemometric methods, as k_2 = 10.7 ± 0.2 L mol^{-1} s^{-1} and k_2' = 0.68 ± 0.05 L mol^{-1} s^{-1}. However, when 1 equiv of dppf is used, the products were found to be different (see Schemes 4, 5, and 6). Thus, again at first a mixture containing complexes **A** and **B** is formed, interestingly with a rate constant value of k_2 = 10.5 ± 0.4 L mol^{-1} s^{-1} similar to that estimated under second-order conditions by UV−visible spectroscopy. Then by the reaction of complex **A** with complex **B**, during which the dangling P atom in complex **A** would attack the platinum center in complex **B**, a new aggregated species, [(*p*-MeC_6H_4)(ppy)Pt(μ-dppf)Pt(*p*-MeC_6H_4)(ppy-κ^1C)(dppf-κ^1P)], **C**, having a dangling dppf ligand, is formed. Attempts to extend the length of aggregation in **C** were not successful and ended with chain breaking.

ASSOCIATED CONTENT

Supporting Information. Crystallographic data in CIF format and details of the chemometric method used for the kinetic study. These materials are available free of charge via the Internet at http://pubs.acs.org.

AUTHOR INFORMATION

Corresponding Author

*E-mail: nabavi@chem.susc.ac.ir (S.M.N.); rashidi@chem.susc.ac.ir (M.R.).

ACKNOWLEDGMENT

We thank the Iran National Science Foundation (Grant No. 87041279) and the Shiraz University Research Council for financial support. We also thank Professor James H. Espenson and Dr. Sirous Jamali for helpful discussions and Mr. Sajedian and Mr. Bijanzadeh for assistance with the multinuclear NMR experiments.

REFERENCES

(1) (a) Togni, A.; Hayashi, T., Ed. *Ferrocenes*; VCH: New York, 1995. (b) Štěpnička, P., Ed. *Ferrocenes: Ligands, Materials and Biomolecules*; John Wiley & Sons Ltd.: England, 2008. (c) Teo, P.; Koh, L. L.; Andy Hor, T. S. *Inorg. Chem.* **2008**, *47*, 9561.

(2) (a) Bandoli, G.; Dolmella, A. *Coord. Chem. Rev.* **2000**, *209*, 161. (b) Sato, M.; Sekino, M.; Akabori, S. *J. Organomet. Chem.* **1988**, *344*, C31. (c) Sato, M.; Shigeta, H.; Sekino, M.; Akabori, S. *J. Organomet. Chem.* **1993**, *458*, 199.

(3) (a) Jamali, S.; Nabavizadeh, S. M.; Rashidi, M. *Inorg. Chem.* **2008**, *47*, 5441. (b) Evans, R. C.; Douglas, P.; Winscom, C. J. *Coord. Chem. Rev.* **2006**, *250* (15−16), 2093. (c) Lu, W.; Mi, B.-X.; Chan, M. C. W.; Hui, Z.; Che, C.-M.; Zhu, N.; Lee, S.-T. *J. Am. Chem. Soc.* **2004**, *126*, 4958. (d) Wong, W.-Y.; He, Z.; So, S.-K.; Tong, K.-L.; Lin, Z. *Organometallic* **2005**, *24*, 4079. (e) Sun, W.; Zhu, H.; Barron, P. M. *Chem. Mater.* **2006**, *18*, 2602. (f) Ravindranathan, D.; Vezzu, D. A. K.; Bartolotti, L.; Boyle, P. D.; Huo, S. *Inorg. Chem.* **2010**, *49*, 8922. (g) Bai, D. R.; Baumgartner, T. *Organometallics* **2010**, *29*, 3289. (h) Mathew, I.; Sun, W. *Dalton Trans.* **2010**, *39*, 5885. (i) Wilson, J. J.; Fedoce Lopes, J.; Lippard, S. J. *Inorg. Chem.* **2010**, *49*, 5303.

(4) (a) Thorn, D. L.; Fultz, W. C. *J. Phys. Chem.* **1989**, *93*, 1234. (b) Smith, D. C.; Haar, C. M., Jr.; Stevens, E. D.; Nolan, S. P. *Organometallics* **2000**, *19*, 1427. (c) Scolaro, L. M.; Plutino, M. R.; Romeo, A.; Romeo, R.; Ricciardi, G.; Belviso, S.; Albinati, A. *Dalton Trans.* **2006**, 2551.

(5) (a) Shahsavari, H. R.; Rashidi, M.; Nabavizadeh, S. M.; Habibzadeh, S.; Heinemann, F. W. *Eur. J. Inorg. Chem.* **2009**, 3814. (b) Ma, J.-F.; Yamamoto, Y. *Inorg. Chim. Acta* **2000**, *299*, 164. (c) Ares, R.; López-Torres, M.; Fernández, A.; Pereira, M. T.; Alberdi, G.; Vázquez-García, D.; Fernández, J. J.; Vila, J. M. *J. Organomet. Chem.* **2003**, *665*, 76. (d) Smyth, D. R.; Hester, J.; Young, V. G., Jr; Tiekink, E. R. T. *CrystEngComm* **2002**, *4*, 517.

(6) (a) Complexes with monodentate dppf ligands are rare, one example being [Co_2(η^1-dppf)(μ_2-(MeO_2C)$_2$$C_2$)(CO)$_5$],[6b] in which the conformation of dppf is "anticlinal eclipsed", with a Cp(centroid)···Fe···Cp(centroid) twist angle of 154.9°. We also have recently suggested the formation of an intermediate complex, [PtMe(ppy)(dppf-κ^1P)], formed during a complicated reaction:[3a] (b) McAdam, C. J.; Duffy, N. W.; Robinson, B. H.; Simpson, J. *J. Organomet. Chem.* **1997**, *527*, 179.

(7) (a) Yeo, W.-C.; Vittal, J. J.; Koh, L. L.; Tan, G. K.; Leung, P.-H. *Organometallics* **2006**, *25*, 1259. (b) Liu, F.; Pullarkat, S. A.; Tan, K.-W.; Li, Y.; Leung, P.-H. *Organometallics* **2009**, *28*, 6254.

(8) Frisch, M. J.; et al. *Gaussian 09*, revision A.02; Gaussian, Inc.: Wallingford, CT, 2009.

(9) Gemperline, P. *Practical Guide to Chemometrics*; CRC: New York, 2006.
(10) del Río, V.; Callao, M. P.; Larrechi, M. S.; de Espinosa, L. M.; Ronda, J. C.; Cádiz, V. *Anal. Chim. Acta* **2009**, *649*, 148.
(11) Thurston, T. J.; Brereton, R. G. *Analyst* **2002**, *127*, 659.
(12) (a) Rashidi, M.; Hashemi, M.; Khorasani-Motlagh, M.; Puddephatt, R. J. *Organometallics* **2000**, *19*, 275. (b) Rashidi, M.; Fakhroeian, Z.; Puddephatt, R. J. *J. Organomet. Chem.* **1991**, *406*, 261. (c) Puddephatt, R. J.; Thomson, M. A. *J. Organomet. Chem.* **1982**, *238*, 231. (d) Nabavizadeh, S. M.; Golbon Haghighi, M.; Esmaeilbeig, A. R.; Raoof, F.; Mandegani, Z.; Jamali, S.; Rashidi, M.; Puddephatt, R. J. *Organometallics* **2010**, *29*, 4893.
(13) *X-AREA Program for the Acquisition and Analysis of Data*, version 1.30; Stoe & Cie GmbH: Darmstadt, Germany, 2005.
(14) *X-RED Program for Data Reduction and Absorption Correction*, version 1.28b; Stoe & Cie GmbH: Darmstadt, Germany, 2005.
(15) *X-SHAPE Program for Crystal Optimization for Numerical Absorption Correction*, version 2.05; Stoe & Cie GmbH: Darmstadt, Germany, 2004.
(16) Sheldrick, G. M. *Acta Crystallogr.* **2008**, *A64*, 112.
(17) (a) Lee, C. T.; Yang, W. T.; Parr, R. G. *Phys. Rev. B* **1988**, *37*, 785. (b) Becke, A. D. *J. Chem. Phys.* **1993**, *98*, 5648. (c) Miehlich, B.; Savin, A.; Stoll, H.; Preuss, H. *Chem. Phys. Lett.* **1989**, *157*, 200.
(18) (a) Hay, P. J.; Wadt, W. R. *J. Chem. Phys.* **1985**, *82*, 270. (b) Wadt, W. R.; Hay, P. J. *J. Chem. Phys.* **1985**, *82*, 284. (c) Roy, L. E.; Hay, P. J.; Martin, R. L. *J. Chem. Theory Comput.* **2008**, *4*, 1029.
(19) Hariharan, P. C.; Pople, J. A. *Theor. Chim. Acta* **1973**, *28*, 213.
(20) Ehlers, A. W.; Böhme, M.; Dapprich, S.; Gobbi, A.; Höllwarth, A.; Jonas, V.; Köhler, K. F.; Stegmann, R.; Veldkamp, A.; Frenking, G. *Chem. Phys. Lett.* **1993**, *208*, 111.
(21) Weigend, F.; Furche, F.; Ahlrichs, R. *J. Chem. Phys.* **2003**, *119*, 12753.